Updated recruitment abundance index of Pacific bluefin tuna based on real-time troll monitoring (RTM) data

Ifue Fukuchi, Yohei Tsukahara, Hiromu Fukuda, Shuya Nakatsuka

Highly Migratory Resources Division, Fisheries Resources Institute,

Japan Fisheries Research and Education Agency

2-12-4, Fukuura, Kanazawa-ku, Yokohama, Kanagawa 236-8648, JAPAN

December 2024

Summary

In this study, we provide an updated real time monitoring (RTM) recruitment index for Pacific bluefin tuna. We reanalyzed the RTM data from Fujioka et al. (2024) by adding the February 2024 data, which was still being collected at the time of PBFWG meeting in March 2024. This reanalysis covered two periods: the entire data collection period from the 2011 to 2023 fishing year, and the period of tightened fishing regulations (i.e., 2017 to the 2023 fishing year). The estimated indices for the most recent year (2023 fishing year) were slightly lower than the previous ones, but the overall trend remained consistent. Additionally, the indices showed a similar trend to those based on traditional sales slip data for the overlapping period (2011 to 2016 fishing years).

Introduction

The recruitment abundance index (i.e. standardized CPUE) based on Japanese troll fishery data was one of the most important input data for the Pacific bluefin tuna (PBF) stock assessment. This index was developed using landing data in certain ports in Nagasaki prefecture in autumn-winter season, which was considered to represent the abundance of recruitment from two spawning grounds (Ichinokawa et al., 2012). Because of the possible change in the catchability (increasing of the penning operation, live release, effect of the catch upper limit), this index was terminated at 2010 fishing year for the stock assessment in 2024 (ISC, 2024).

Because troll sales slip data was strongly affected by fishing regulations and the fishing operation, the RTM survey index was submitted to the PBFWG as a candidate for alternative recruitment index (Fujioka et al., 2021, 2022, 2023, 2024). The RTM data provides geographic information on operations by vessels, allowing us to aggregate catch and effort data into a

detailed latitude-longitude grids. Another advantage of the RTM data is that live release data and zero-catch operations can be obtained in a spatiotemporally fine-grained and timely manner (Tsukahara et al., 2019, Nishikawa et al., 2021). Since 2021 fishing year, scientific surveys using chartered RTM vessels have been conducted in the same time and space as conventional RTM. Because this survey is independent from the Individual Quota management, it would ensure to obtain more robust data to the changes is fishing regulations.

In this study, we added the February 2024 data, which was still being collected at the time of the stock assessment meeting held at March 2024, and estimated recruitment indices for the entire period of data collection from 2011 to 2023 fishing year, as well as for the period of tightened fishing regulations (i.e. 2017 to 2023 fishing year).

Methods

Data collection and summary

The dataset used for reanalysis in this study is the same as Fujioka et al. (2023), except for the catch and effort data in February 2024. Data from 14 RTM vessels, which targeted for age-0 PBF (i.e. 40-60 cm fork length) during the winter season (November to following February) in the East China Sea (ECS), have been collected since 2011 fishing year. The RTM data were collected in the same season and area as the traditional troll indices (sales slip basis) which represents the abundance of juvenile PBF born in both main spawning grounds in the North Western Pacific Ocean and the Sea of Japan. Locations of fishing port for those RTM vessels are shown in Figure 2. The number of RTM vessels increased to 14 vessels to date, and operational data were collected from 7 to 14 vessels each fishing year (Fig. 3). This paper updates the operational data by 14 vessels for the analysis period of 2011-2023 fishing year (Table 1). Since

2021 fishing year, in addition to conventional RTM, those conventional 14 RTM vessels were chartered for 10 days from November through February with at least one operation in each month to secure operations in the monitoring period, namely chartered RTM. They can operate independently with IQ as the catch from chartered operations were reported as part of the national government authorized FRA survey quota. Unless otherwise noted, the data from chartered RTM is included in the analysis.

RTM vessels are equipped with the GPS receiver and numeric keypad to input species and number of fish caught at the fishing location. The GPS data is recorded at intervals of 1 second during all trips. The vessel velocity can be estimated by the moving distance based on the GPS data. The estimated velocity was smoothed by the trimmed mean to exclude the obvious outlier due to the unsettled GPS data. These trace of fishing behavior and catch position can be used to estimate more precise efforts in an operation, i.e., actual operation time, than the catch per day used for sales slip data in the original index. PBF operation was defined as continuous vessel's velocity in the range of 2-7 knot for more than 30 minutes. The PBF catch and effort (residence time in minutes) data were aggregated in a 0.1×0.1 degree latitude/longitude grids and formatted into the following data; vessel name, year, month, day, latitude, longitude, catch, effort.

Data was carefully reviewed and any operations that were not clearly PBF operations based on the vessel's track and location records was removed by expert judgement. This is because fishermen may operate targeting other fish species due to changes in the catchability of PBF and/or demand for farming depending on year and season. We also excluded data that had obvious errors in the numeric keypad entry on board (e.g., more than 500 catches in one operation). Also, data in the northeastern part of Tsushima (latitude >34.5, longitude >129.2) was excluded (38 grids) because it was a unique fishing ground only for the 2011 fishing year (Fujioka et al. 2021). This kind of data in rarely sampled area may affect the estimation of

spatial effect of whole time series by the nature of VAST model for sharing information over space and time.

The spatial distribution of RTM operations by year is shown in Figure 4. Histograms of fishing effort (in minutes) and PBF catch records from 2011 to 2023 are shown in Figure 5. For the 0.1 degree grid aggregated data, the mean and standard deviation for fishing effort was 102.7 ± 105.0 minutes, ranging from 5 to 735 minutes. The mean and standard deviation of PBF catch in each area was 3.6 ± 11.4 with a range of 0 to 284. For the entire period (2011-2023), the zero-catch rate operation was 66%, the positive catch rate was 34%, and the coefficient of variation of PBF catch (S.D./Mean) was 3.17. Nominal CPUE for each month and fishing year is shown in Figure 6.

Vector Autoregressive Spatio-Temporal (VAST) model

VAST is a delta-generalized linear mixed model that separately calculates the encounter probability and the positive catch rate, and is available from the R package "VAST" version 3.11.2 on the website (https://github.com/James-Thorson-NOAA/VAST) (Thorson, 2019). In our study, the encounter probability (p) at observation i was modeled using a logit-linked linear predictor, and the positive catch rate (r) at observation i was modeled using a log-linked linear predictor, as in the following equation:

(1) $\text{logit}(p_i) = \beta_1(t_i) + L_{\omega 1}\omega_1(s_i) + L_{\varepsilon 1}\varepsilon_1(s_i, t_i) + \zeta_1(s_i, m_i) + L_{\eta 1}\eta_1(v_i)$

(2) $\log(r_i) = \beta_2(t_i) + L_{\omega 2}\omega_2(s_i) + L_{\varepsilon 2}\varepsilon_2(s_i, t_i) + \zeta_2(s_i, m_i) + L_{\eta 2}\eta_2(v_i)$

where $\beta(t_i)$ is the intercept in year t_i, $\omega(s_i)$ is the time-invariant spatial variations at location s_i, $\varepsilon(s_i, t_i)$ is the time-varying spatio-temporal variations at location s_i in year t_i,

$\zeta(s_i, m_i)$ is the s_i month effect m_i as a catchability covariate which is either spatially varying at location at s_i or spatially constant by configuration and $\eta(v_i)$ is the effect of vessel v_i as a factor of overdispersion, and L_ω, L_ε and L_η are the scaling coefficients of the random effect distributions (Fujioka et al., 2021, 2022, 2023, 2024).

The probability of the density *c* is specified in this study as follows for a zero-inflated Poisson distribution:

$$(3)\quad \Pr(c_i = c) = \begin{cases} 1 - p_i & \text{if } c = 0 \\ p_i \times ZeroInflated\ Poisson(c_i|\log(r_i), \sigma^2) & \text{if } c > 0 \end{cases}$$

where σ^2 is a dispersion parameter.

Then, the abundance index was predicted using an area-weighted approach, which calculates total abundance as a weighted sum of the estimated densities in a pre-defined spatial domain of knots. The number of knots was set equal to the number of observation locations (223 knots for 2011-2023).

Regarding the configuration of spatial structure with Gaussian Random Markov field (GRMR), this analysis used the anisotropic estimation of correlation, which estimate two different parameters for the correlation of two independent directions. In terms of temporal configuration, there is no assumption of correlated structure both year effect itself and spatio-temporal variation because the recruitment strength was highly variable over years based on the PBF assessment result.

In this study, we added one-month data (Feb 2024) and conducted reanalysis for both periods using Case 5 from Fujioka et al. (2024), which had the lowest AIC value. This case assumed spatial and spatio-temporal effects, with the month effect as a catchability covariate that varied spatially for each of encounter probability.

Results and Discussion

This study provides the RTM recruitment index with updated data for February 2024 to the dataset analyzed in Fujioka et al. (2024). The additional data includes 87 operational days, in which 20 days were from chartered vessels and the rest of days were from conventional monitoring (Table 2). The standardized CPUE for February 2024 was 0.056, which was lower than January 2024 but still not a particularly low value in overall (Fig. 6). In the two periods from 2011 to 2023 and from 2017 to 2023, the final gradient values for each parameter were sufficiently low, indicating successful convergence (Tables 3-1, 3-2). The quantile diagnostics did not show any significant negative signs in the standardization (Figs. 11-1, 11-2). The spatiotemporal distribution of the log-transformed predicted density of PBF analyzed by the VAST model is shown in Figures 7-1 and 7-2, respectively. Both periods reflect recent strong recruitment strength, and overall high densities are expected in recent years. The decorrelation distances in different directions for encounter probability and positive catch rate are shown in Figures 8-1 and 8-2. The center of gravity of recruitment, indicating changes in the east-west and north-south distribution during the survey period, is shown in Figures 9-1 and 9-2. The standardized index of relative abundance in 2023 was higher than the previous year, with a slightly reduced distribution range (Figs. 10-1, 10-2). Although the index in this study was slightly lower than that of Fujioka et al. (2024) in recent years, the overall trends were very similar in both periods. Additionally, the trends were similar during the overlapping period (2011-2016) with the sales slip data (Fig. 12).

This study updated the recruitment index for the fishing year 2023 by adding data from February 2024 to the dataset used by Fujioka et al. (2024). Continuous data collection based on

this kind of survey is essential, and further research on the possible targeting effect, environmental effect, migration of fish will make the recruitment index based on RTM data more reliable. In near future, we plan to examine in detail the differences in CPUE between chartered RTM and conventional RTM.

References

Fukuda, H., Fujioka, K., Tsukahara, Y., Nishikawa, K. and Nakatsuka, S. 2021. Reinforcement of Japanese PBF recruitment monitoring program. ISC/21/PBFWG-1/06.

Fujioka, K., Tsukahara, Y., Asai, S., Nishikawa, K., Fukuda, H. and Nakatsuka, S. 2021. Estimation of recruitment index of Pacific bluefin tuna based on real-time troll monitoring survey data using Vector Autoregressive Spatio-Temporal (VAST) model analysis. ISC/21/PBFWG-02/03.

Fujioka, K., Tsukahara, Y., Asai, S., Fukuda, H. and Nakatsuka, S. 2022. Update of estimated recruitment index of Pacific bluefin tuna based on real-time troll monitoring survey data, added IQ-independent scientific survey data for 2021. ISC/22/PBFWG-02/01.

Fujioka, K., Tsukahara, Y., Asai, S., Fukuda, H. and Nakatsuka, S. 2023. Recruitment abundance index of immature Pacific bluefin tuna, derived from real-time monitoring survey data of troll fisheries. ISC/23/PBFWG-01/03.

Fujioka, K. Asai, S., Tsukahara, Y., Fukuda H. and Nakatsuka, S. 2024 Recruitment abundance index of Pacific bluefin tuna based on real-time troll monitoring survey data using Vector Autoregressive Spatio-Temporal (VAST) model analysis. ISC/24/PBFWG-1/04

Ichinokawa, M., Oshima, K. and Takeuchi, Y. 2012. Abundance indices of young Pacific bluefin tuna, derived from catch-and-effort data of troll fisheries in various regions of Japan. ISC/12/PFWG-1/11.

ISC 2022. Report of the Pacific bluefin tuna working group intersessional workshop. ISC/22/ANNEX/06.

ISC 2024. Stock assessment of pacific blue fin tuna in the pacific ocean in 2024.

ISC/24/ANNEX/13

Nishikawa, K., Tsukahara, Y., Fujioka, K., Fukuda, H. and Nakatsuka, S. 2021. Update of age-0 PBF index based on catch per unit effort data from Japanese troll fishery and its associated issues. ISC/21/PFWG-1/05.

Thorson, JT. 2019. Guidance for decisions using the Vector Autoregressive Spatio-Temporal (VAST) package in stock, ecosystem, habitat and climate assessments. *Fish. Res.* 210: 143-161.

Tsukahara, Y. and Chiba, K. 2019. Real-time recruitment monitoring for Pacific bluefin tuna using CPUE for troll vessels: Update up to 2018 fishing year. ISC/19/PBFWG-1/04.

Table 1 (a) Total number of efforts (in days) and (b) number of latitude/longitude grids (in 0.1 grid units) by 7-14 real-time troll monitoring vessels per month from 2011 to 2023 FY.

a)	Total number of troll operations (days)												
	2011	2012	2013	2014	2015	2016	2017	2018	2019	2020	2021	2022	2023
November	31	67	27	42	113	64	57	67	35	30	90	49	23
December	99	93	67	71	163	53	39	112	88	49	165	76	92
January	58	58	110	120	107	80	0	132	176	30	114	99	92
February	74	0	90	20	115	74	0	120	107	23	121	81	87
Total	262	218	294	253	498	271	96	431	406	132	490	305	294

b)	Total number of troll operations (grids)												
	2011	2012	2013	2014	2015	2016	2017	2018	2019	2020	2021	2022	2023
November	22	30	29	27	43	31	24	31	25	25	48	26	22
December	50	64	40	54	75	40	30	28	30	36	69	46	45
January	68	68	71	91	42	38	0	62	30	32	59	44	41
February	64	0	63	36	52	62	0	63	44	29	38	49	35
Total	204	162	203	208	212	171	54	184	129	122	214	165	78

Table 2 Monthly effort (in days) and grid (in 0.1 grid units) of conventional real-time monitoring and chartered real-time monitoring by 14 troll vessels in the 2023 FY. Both monitoring surveys were conducted by the same 14 troll vessels.

	Total operation		Conventonal		Charter		Ratio of chater to conventonal	
	days	grids	days	grids	days	grids	days (%)	grids (%)
November	23	22	8	10	15	12	187.5	120.0
December	92	45	50	27	42	31	84.0	114.8
January	92	41	52	31	40	23	76.9	74.2
February	87	35	67	27	20	21	29.9	77.8
Total	294	143	177	95	117	87	66.1	91.6

Table 3-1 Initial and final condition of each parameter related to explanatory variables in the 2011-2023 FY period. The list of parameters is as follows: beta; intercept for 1st or 2nd linear predictor (1st; encounter probability, 2nd; positive catch rate) each fishing year (2011-2023), L_omega; spatial factors for 1st or 2nd linear predictor, L_epsilon; spatio-temporal factors for 1st or 2nd linear predictor, logkappa; decorrelation rate for 1st or 2nd linear predictor, log_sigmaPhi; conditional variance between each month for intercepts of 1st linear predictor

Parameter	Starting value	Lower boundary	Maximum likelihood estimation	Upper boundary	Final gradient
ln_H_input	-0.122480467	-5	-0.122486505	5	-4.68E-10
ln_H_input	-0.026909552	-5	-0.026933517	5	-8.94E-11
beta1_ft	-0.497060774	-Inf	-0.496994765	Inf	3.32E-09
beta1_ft	-1.083040606	-Inf	-1.08303062	Inf	-9.04E-10
beta1_ft	-0.50504634	-Inf	-0.504941597	Inf	6.90E-09
beta1_ft	-0.976061378	-Inf	-0.976010873	Inf	2.23E-09
beta1_ft	-0.603423996	-Inf	-0.603401714	Inf	4.58E-11
beta1_ft	0.495487652	-Inf	0.495515434	Inf	-1.48E-10
beta1_ft	0.590563524	-Inf	0.590612844	Inf	1.92E-09
beta1_ft	-0.270338727	-Inf	-0.270303762	Inf	6.81E-10
beta1_ft	-0.908387153	-Inf	-0.908351406	Inf	1.01E-09
beta1_ft	-0.672919538	-Inf	-0.67288342	Inf	9.38E-10
beta1_ft	0.500064543	-Inf	0.500001835	Inf	-8.81E-09
beta1_ft	0.640000918	-Inf	0.639996904	Inf	-2.85E-09
beta1_ft	0.736434766	-Inf	0.736401576	Inf	-3.74E-09
L_omega1_z	-1.020042414	-Inf	-1.020055341	Inf	8.08E-09
L_epsilon1_z	-0.793933441	-Inf	-0.793919336	Inf	1.06E-07
logkappa1	-2.888416624	-4.790245443	-2.888390754	-1.173741756	8.37E-08
log_sigmaPhi1_k	-0.646464235	-Inf	-0.646533565	Inf	1.87E-08
log_sigmaPhi1_k	-0.483764703	-Inf	-0.483686692	Inf	1.71E-08
log_sigmaPhi1_k	-0.077585068	-Inf	-0.077628962	Inf	1.41E-09
beta2_ft	-3.358430244	-Inf	-3.358435404	Inf	-6.65E-10
beta2_ft	-3.486658678	-Inf	-3.486642351	Inf	3.43E-10
beta2_ft	-2.92086042	-Inf	-2.920836882	Inf	2.53E-09
beta2_ft	-4.314991992	-Inf	-4.314973953	Inf	1.66E-09
beta2_ft	-3.895216106	-Inf	-3.89522066	Inf	-1.63E-09
beta2_ft	-3.138494418	-Inf	-3.138482936	Inf	7.29E-10
beta2_ft	-2.873399839	-Inf	-2.873377859	Inf	1.77E-09
beta2_ft	-2.863983141	-Inf	-2.864017205	Inf	-4.05019E-09
beta2_ft	-3.446144484	-Inf	-3.446151133	Inf	-1.42163E-09
beta2_ft	-3.453255825	-Inf	-3.453232818	Inf	1.53518E-09
beta2_ft	-2.634960868	-Inf	-2.634925723	Inf	3.35194E-09
beta2_ft	-3.249419028	-Inf	-3.249340034	Inf	6.65682E-09
beta2_ft	-2.543365627	-Inf	-2.543390591	Inf	-3.01398E-09
L_omega2_z	0.347028646	-Inf	0.347031338	Inf	-1.67011E-08
L_epsilon2_z	-0.830011971	-Inf	-0.830012073	Inf	9.36344E-08
logkappa2	-1.970361579	-4.790245443	-1.97039002	-1.173741756	2.22515E-08
log_sigmaPhi2_k	-0.433068669	-Inf	-0.433090937	Inf	-2.86827E-09
log_sigmaPhi2_k	-0.377612624	-Inf	-0.37760733	Inf	-2.42906E-09
log_sigmaPhi2_k	-0.316833674	-Inf	-0.316827437	Inf	-1.59025E-09

Table 3-2 Continuing with the dataset for the period 2017-2023 FY.

Parameter	Starting value	Lower boundary	Maximum likelihood estimation	Upper boundary	Final gradient
ln_H_input	-0.166789982	-5	-0.166793203	5	5.26E-09
ln_H_input	-0.010824604	-5	-0.01083139	5	6.68E-09
beta1_ft_2017	0.276429902	-Inf	0.276500157	Inf	-3.89E-10
beta1_ft_2018	-0.37829038	-Inf	-0.378288632	Inf	5.30E-10
beta1_ft_2019	-0.97706726	-Inf	-0.977065742	Inf	2.34E-10
beta1_ft_2020	-0.747726419	-Inf	-0.74772421	Inf	3.51E-10
beta1_ft_2021	0.520671853	-Inf	0.520572296	Inf	-6.93E-10
beta1_ft_2022	0.675189648	-Inf	0.675225034	Inf	-9.62E-10
beta1_ft_2023	0.520798206	-Inf	0.52086744	Inf	2.85E-10
L_omega1_z	-1.031575567	-Inf	-1.031537705	Inf	6.61E-09
L_epsilon1_z	-0.920660671	-Inf	-0.920643915	Inf	4.56E-08
logkappa1	-2.852450271	-4.766133086	-2.852430436	-1.174944988	2.20E-08
log_sigmaPhi1_k	-0.645379378	-Inf	-0.645344114	Inf	3.05E-09
log_sigmaPhi1_k	-0.201113362	-Inf	-0.201136929	Inf	3.75E-10
log_sigmaPhi1_k	0.005143812	-Inf	0.005091556	Inf	7.00E-10
beta2_ft_2017	-2.924078864	-Inf	-2.924113119	Inf	2.46E-09
beta2_ft_2018	-2.451521137	-Inf	-2.451463983	Inf	-4.40E-09
beta2_ft_2019	-3.563039987	-Inf	-3.563053811	Inf	2.24E-10
beta2_ft_2020	-3.6115274	-Inf	-3.611592872	Inf	3.62E-09
beta2_ft_2021	-2.70808792	-Inf	-2.708087481	Inf	-1.11E-09
beta2_ft_2022	-3.284351832	-Inf	-3.28442841	Inf	8.67E-09
beta2_ft_2023	-2.488956999	-Inf	-2.488954147	Inf	-8.33E-10
L_omega2_z	0.435809498	-Inf	0.435816703	Inf	-1.59E-08
L_epsilon2_z	0.99908578	-Inf	0.999090639	Inf	-6.68E-08
logkappa2	-2.450587964	-4.766133086	-2.45059381	-1.174944988	4.20E-09
log_sigmaPhi2_k	-0.159931766	-Inf	-0.15990904	Inf	-4.90E-10
log_sigmaPhi2_k	0.088284528	-Inf	0.088310304	Inf	-2.58E-10
log_sigmaPhi2_k	-0.112281221	-Inf	-0.112270046	Inf	-2.90E-09

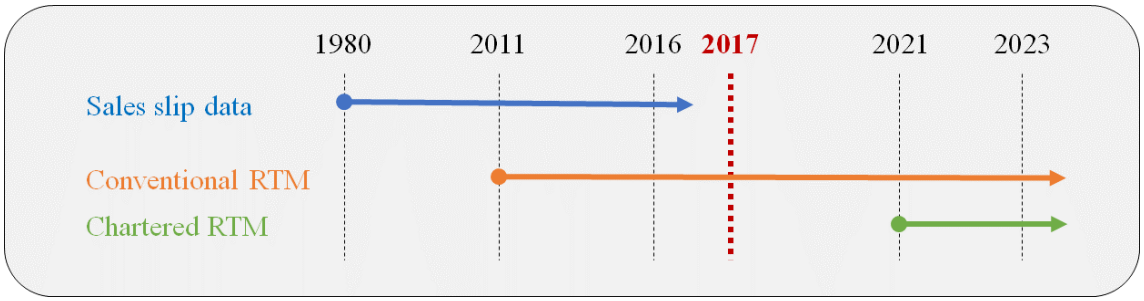

Figure 1 Three types of data collection of age-0 PBF from troll fisheries from 1980 to 2023 fishing year. The conventional real-time monitoring (RTM) and chartered RTM began in the 2011 and 2021 FY, respectively.

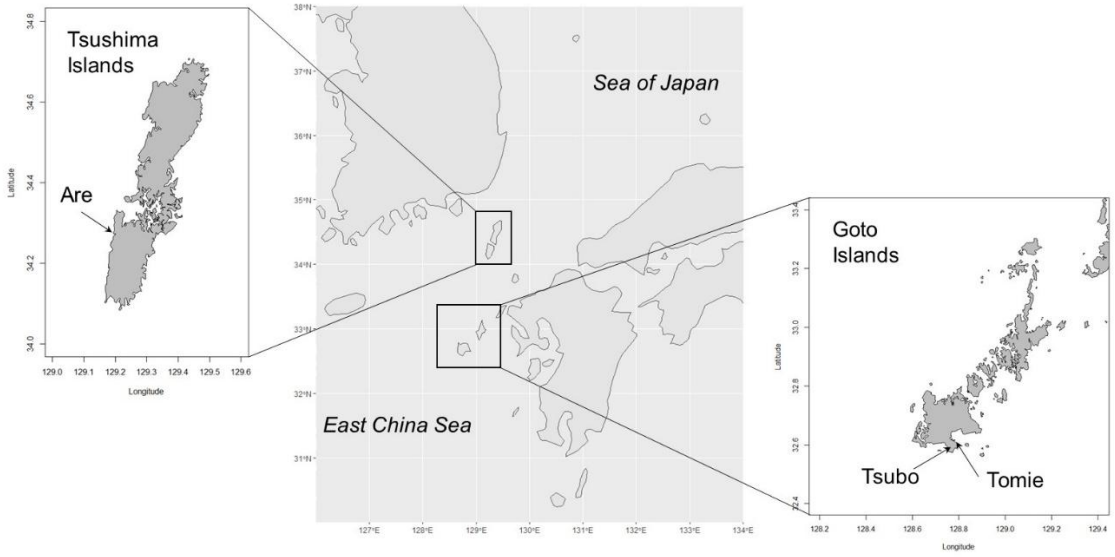

Figure 2 Location of fishing ports where real-time monitoring data of troll fisheries have been collected in Nagasaki prefecture. Left: 5 vessels in Izuhara-Are, Tsushima Islands. Right: 5 vessels in Goto-Tomie, and 4 vessels in Goto-Tsubo, Goto Islands.

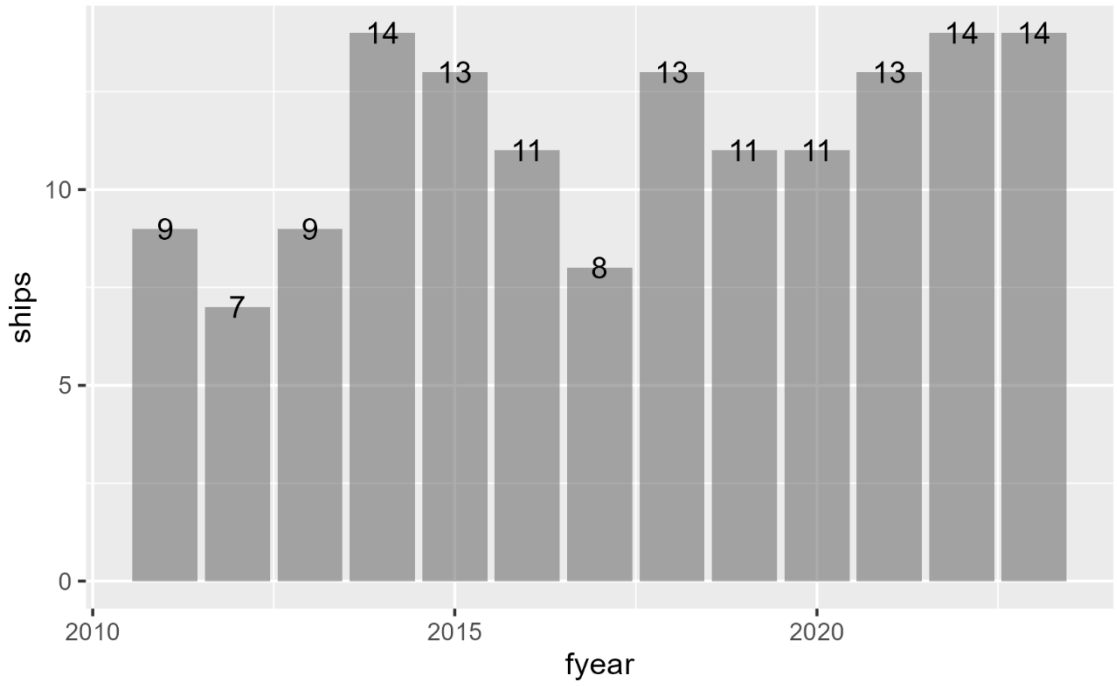

Figure 3 The number of real-time monitoring vessels with PBF operations from 2011 to 2023 FY.

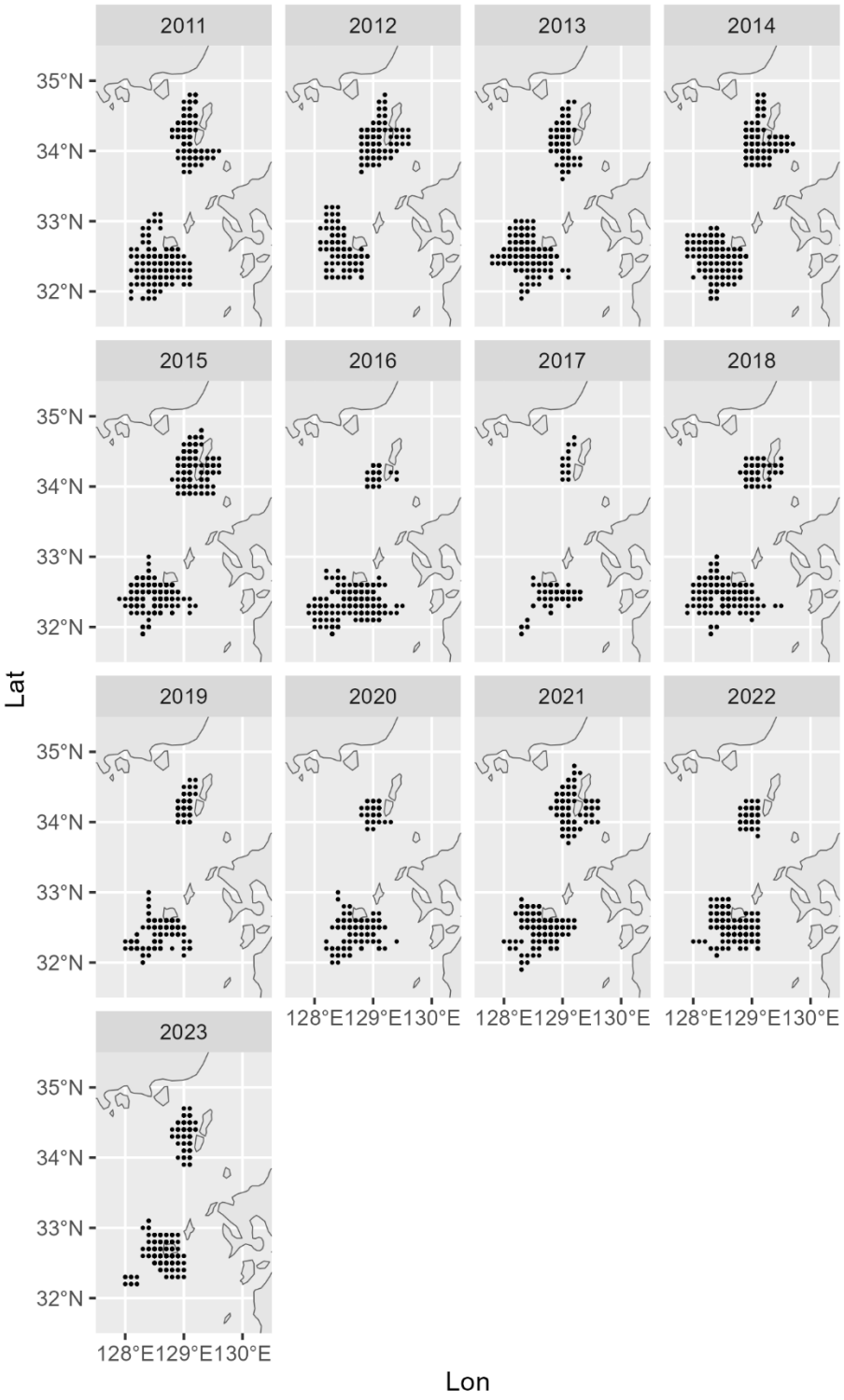

Figure 4 Distribution of troll operations of 7-14 real-time monitoring vessels from 2011 to 2023 FY.

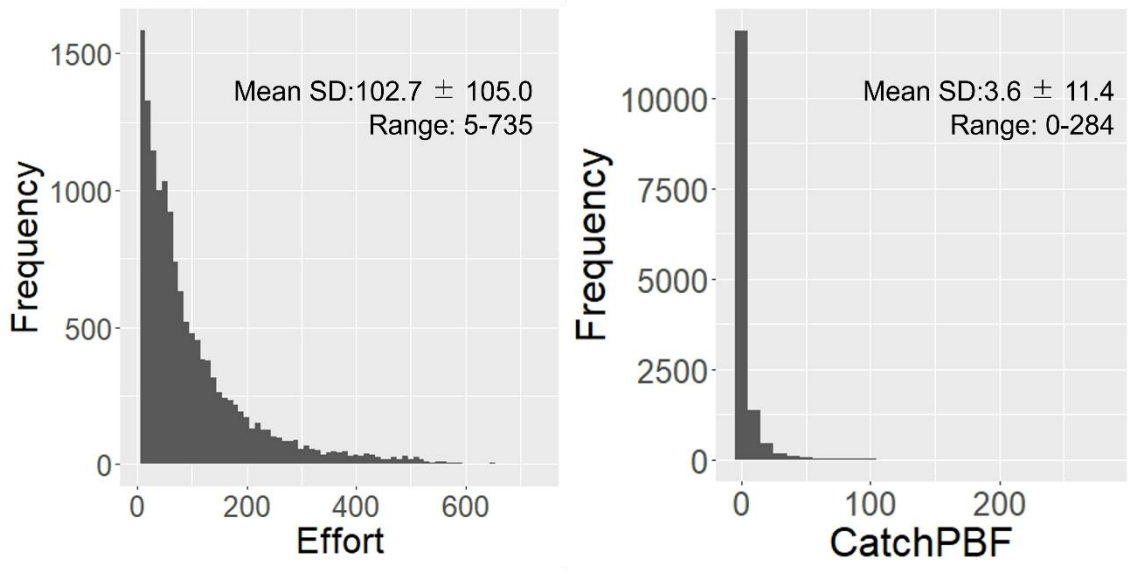

Figure 5 Frequency of fishing efforts (left) and PBF catches (right) for 2011-2023 FY based on 0.1 degree grid aggregate data.

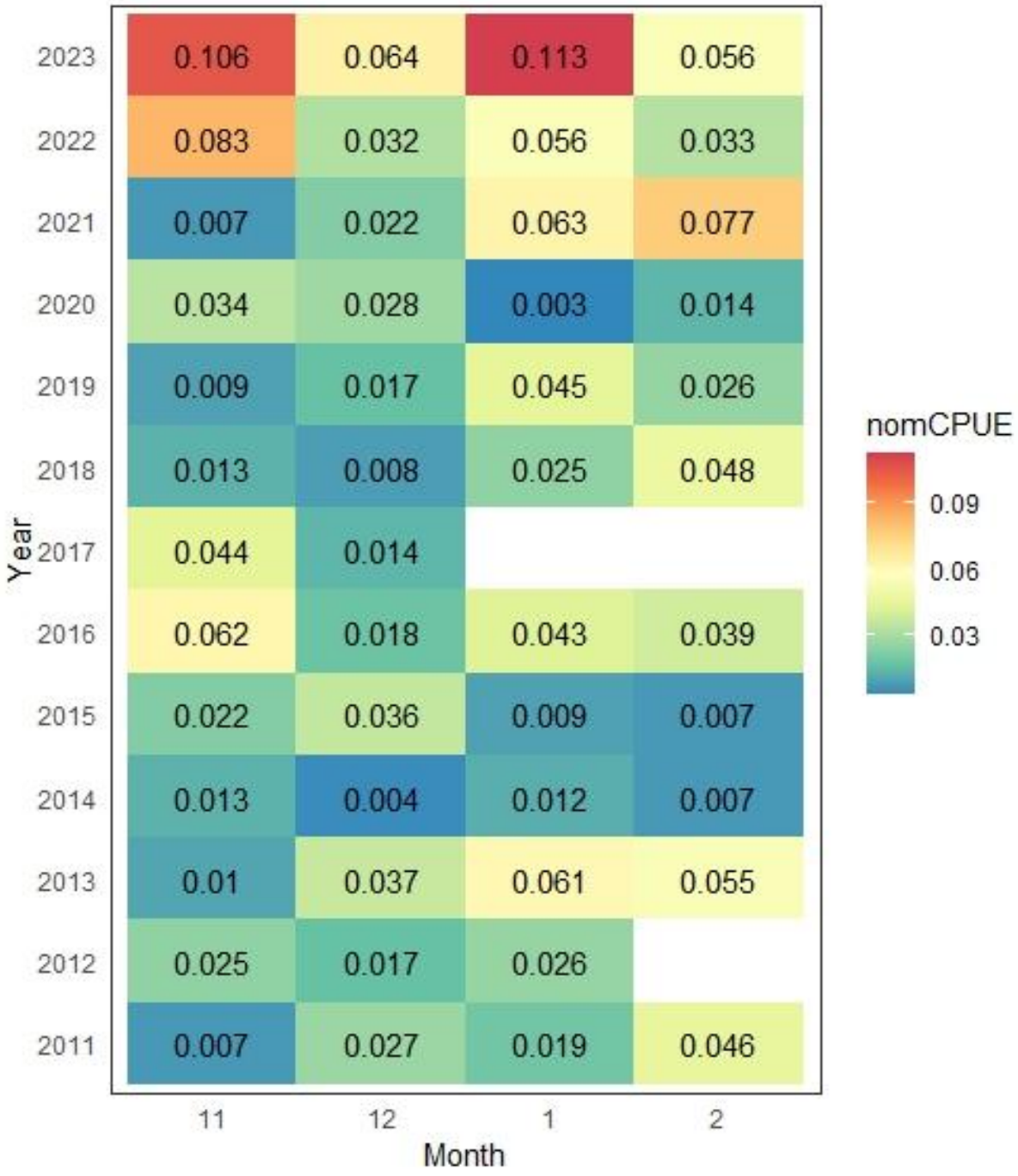

Figure 6 Nominal CPUE during 2011-2023 FY for each month (November to following February). No operations during the months of January and February of 2017 due to fishing regulations.

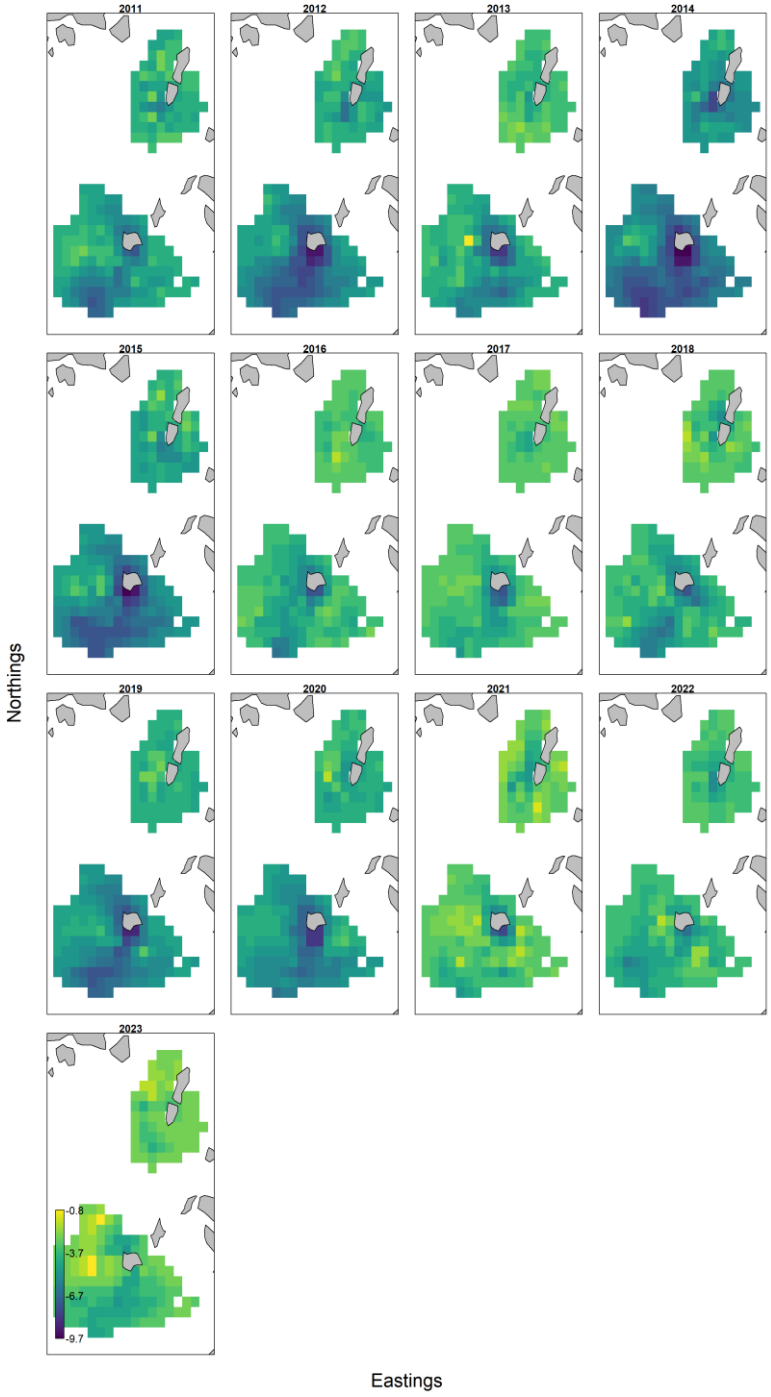

Figure 7-1 Spatio-temporal distribution of the log-transformed predicted densities of PBF for the 2011-2023 FY analyzed by VAST model. Warmer and cooler colors indicate high and low values, respectively.

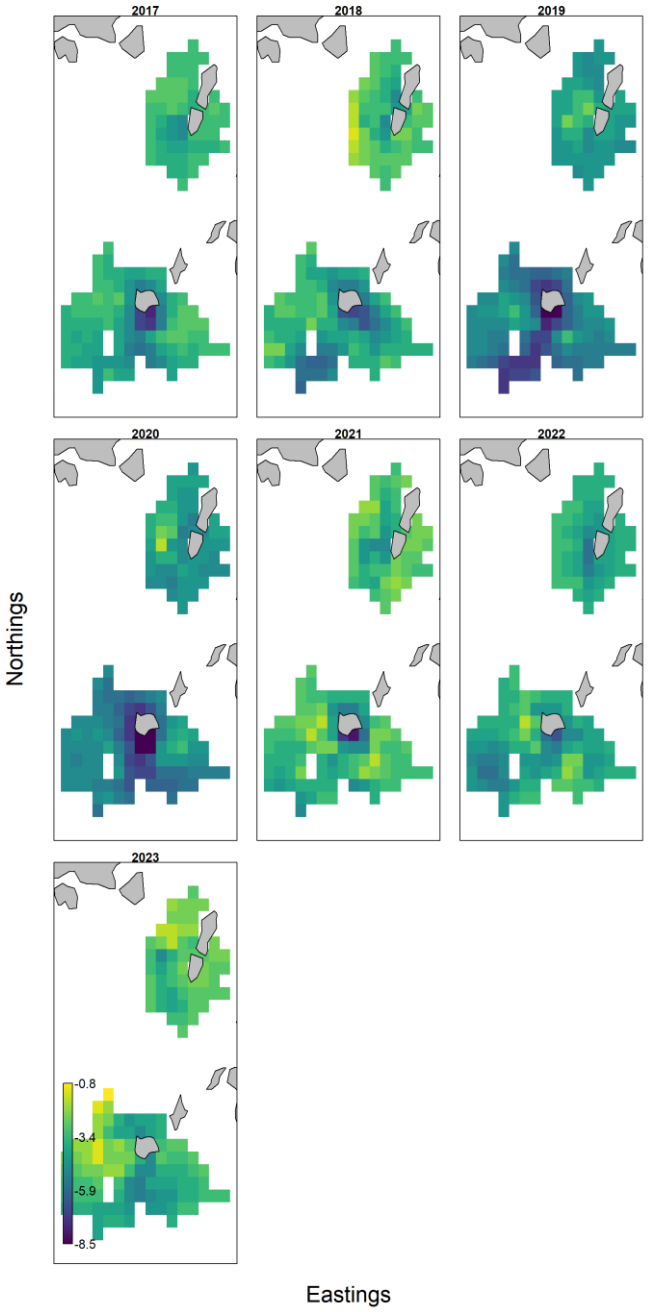

Figure 7-2 Continuing with the dataset for the period 2017-2023 FY.

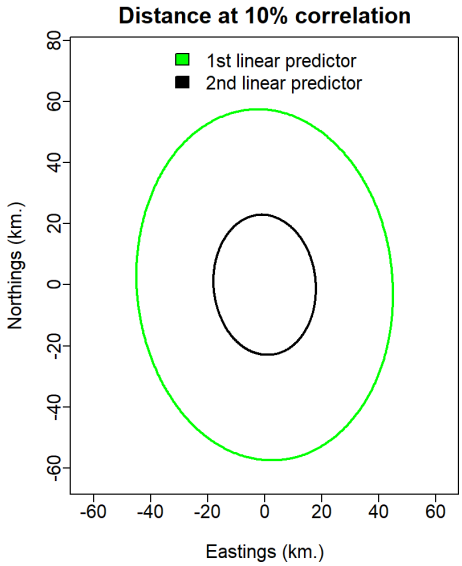

Figure 8-1 Decorrelation distance for different directions relative to encounter probability and positive catch rate for each of the two data periods 2011-2023 FY. Indicating the magnitude of 2-dimensional spatial autocorrelation, and the ellipse signifies the distance (from a point located at position (0,0)), where the correlation drops to 10 %. The predicted densities correlated over a longer distance in the north-south direction than in the east-west direction.

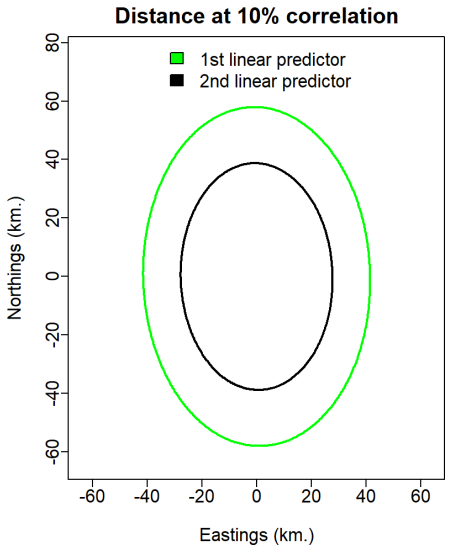

Figure 8-2 Continuing with the dataset for the period 2017-2023 FY.

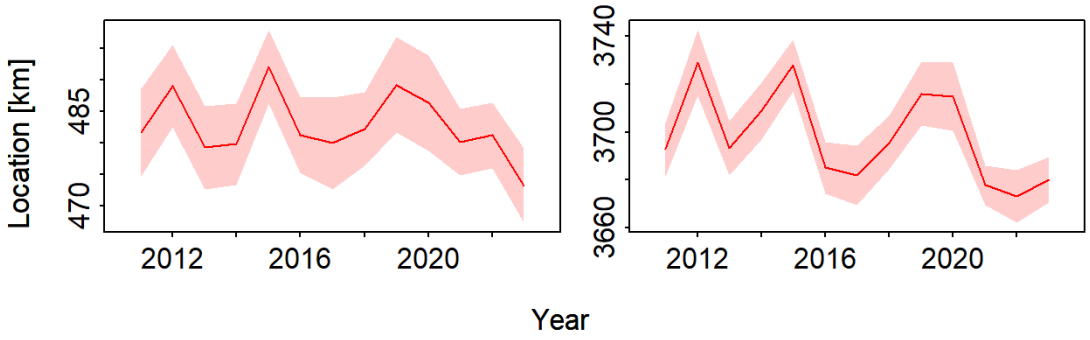

Figure 9-1 The center of gravity of PBF recruitments indicating the shift in distribution (distance (km)) in the east-west (left) and north-south (right) directions for the periods of 2017-2023 FY. The thick line with shading indicates the mean value and standard error.

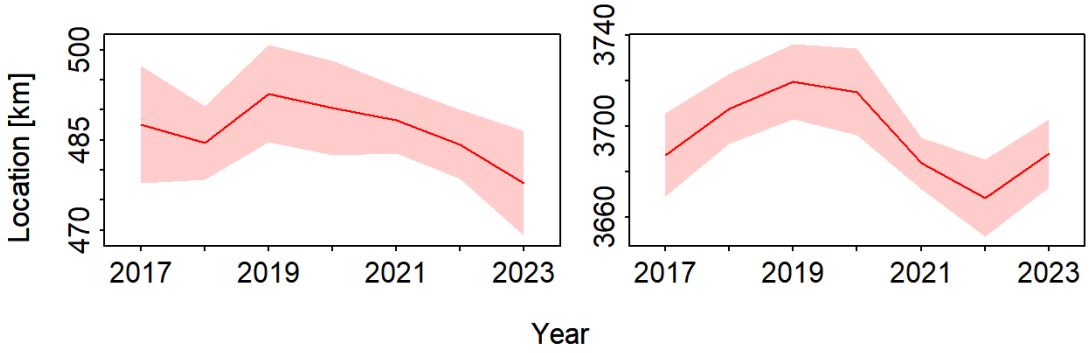

Figure 9-2 Continuing with the dataset for the period 2017-2023 FY.

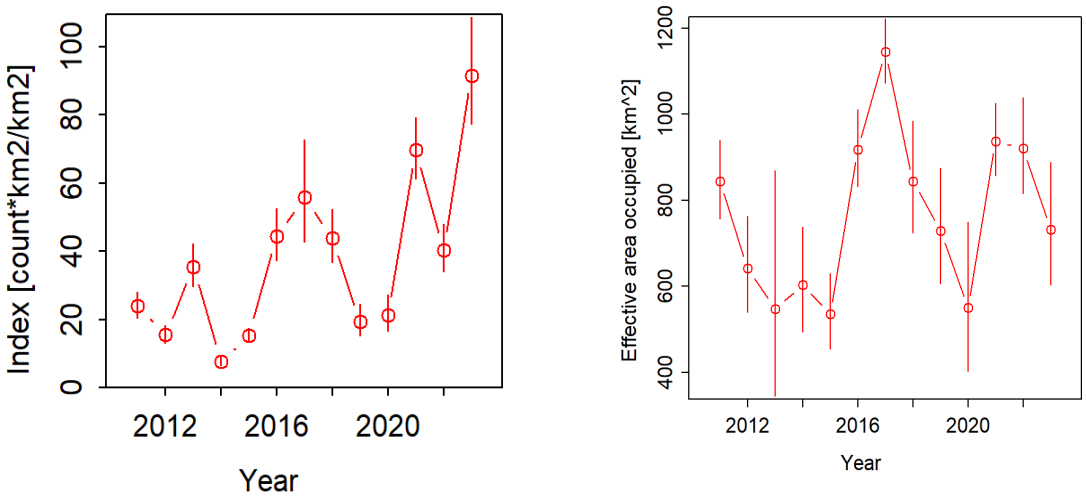

Figure 10-1 Standardized index of relative abundance of PBF (left) and estimated of the effective area occupied by PBF indicating range expansion/contraction (right) for the periods of 2011-2023 FY. The open circles with vertical lines denote point estimates with standard errors.

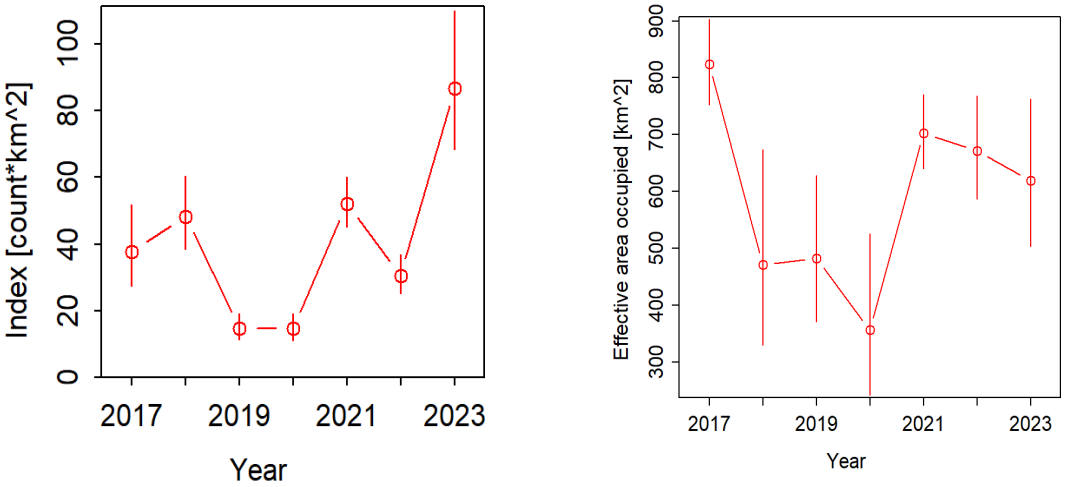

Figure 10-2 Continuing with the dataset for the period 2017-2023 FY.

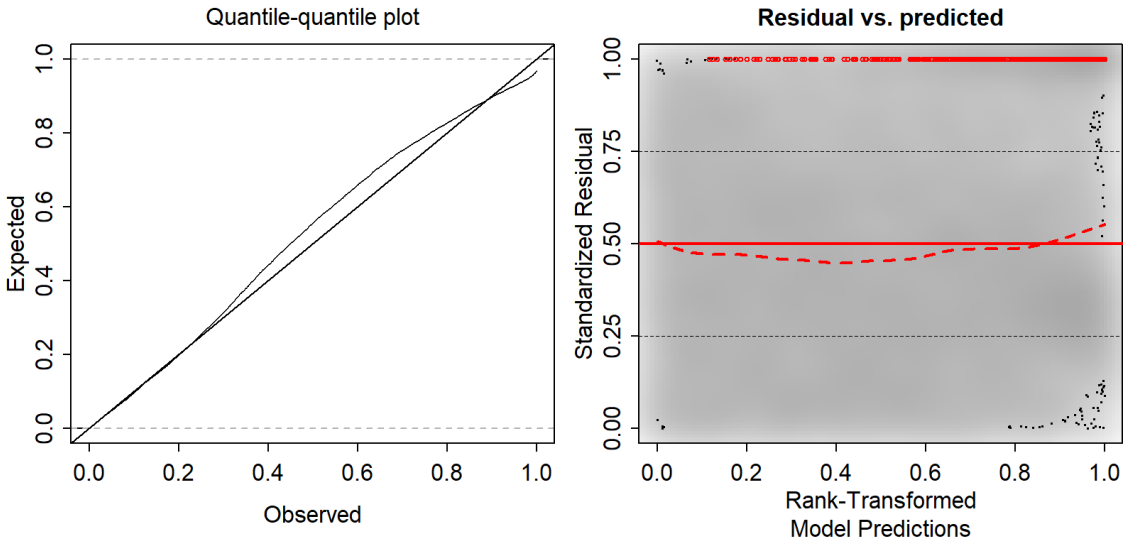

Figure 11-1 Diagnostic Q-Q plot (left) and residual plots (right) comparing the observed and predicted quantiles for the periods of 2011-2023 FY. The residual plot calculating a quantile regression to compare the empirical 0.5 quantile in y-direction (dashed red lines) with the theoretical 0.5 quantile (red solid line).

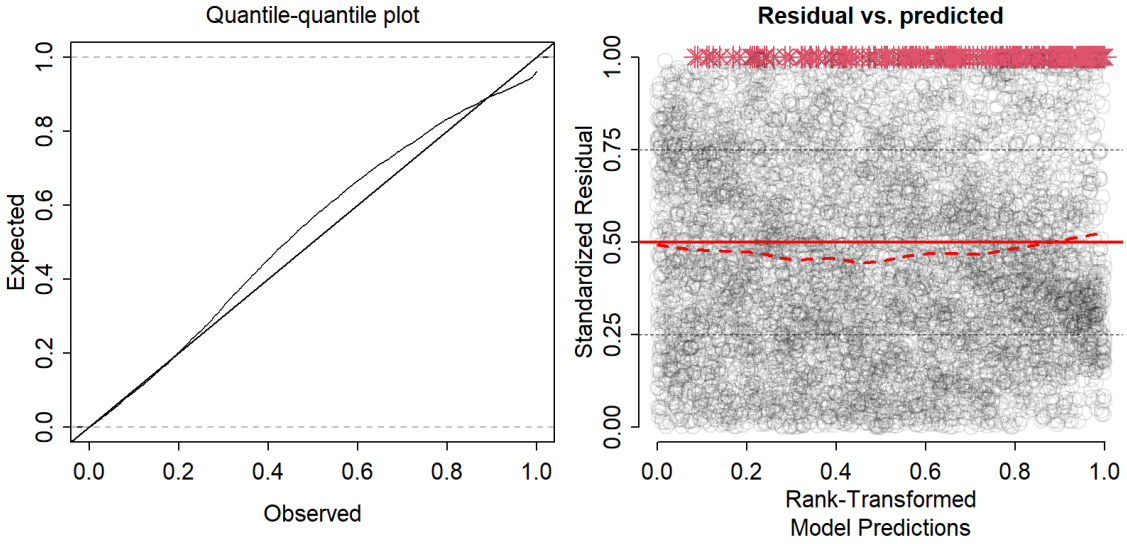

Figure 11-2 Continuing with the dataset for the period 2017-2023 FY.

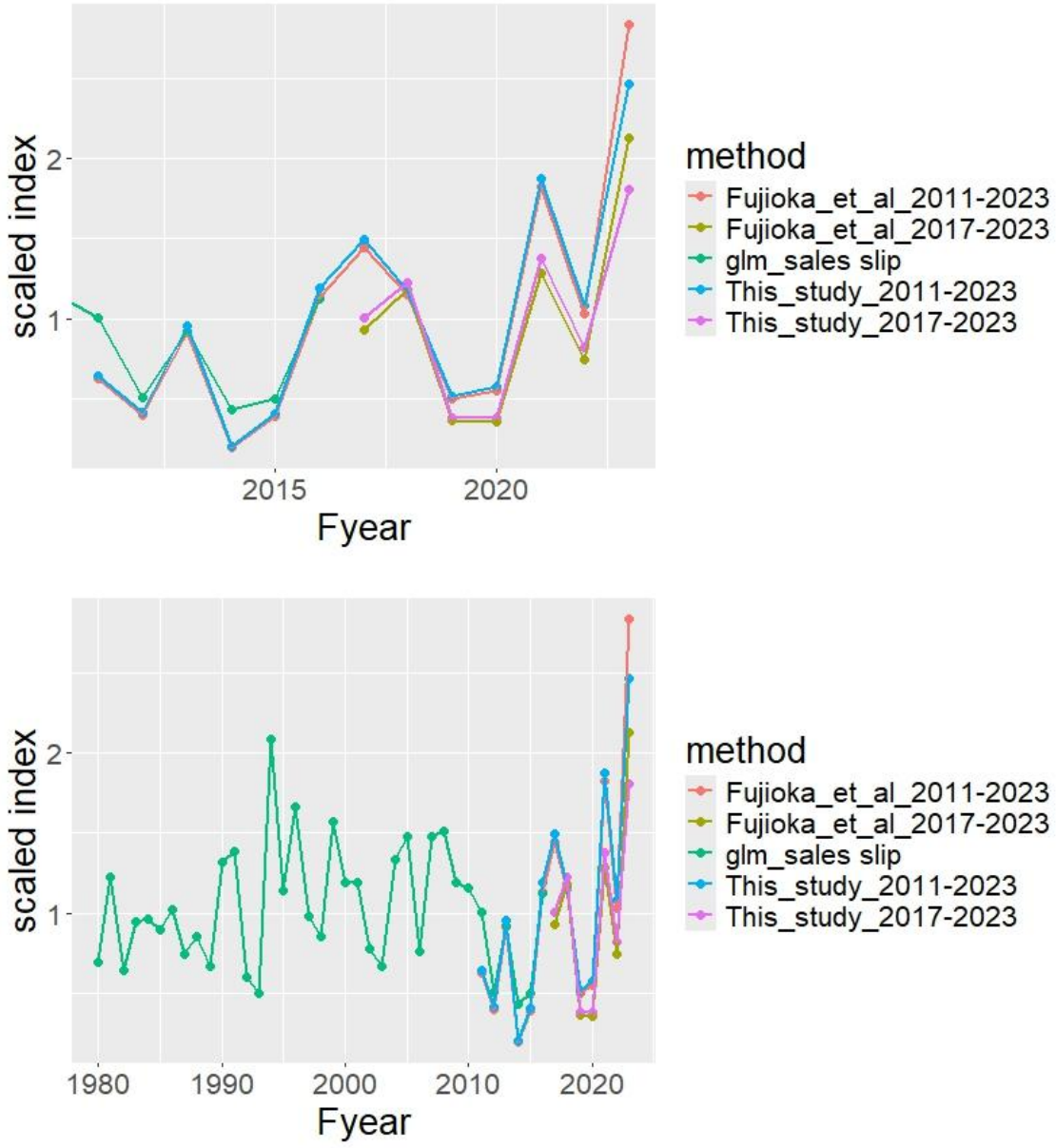

Figure 12 Recent trends of scaled abundance indices on results both traditional GLM (green line) using sales slip data (Nishikawa et al., 2021), VAST analyses using real-time monitoring data for the periods November 2011- January 2023 FY (red line), November 2017 FY- January 2023 FY (brown line) (Fujioka et al., 2023), November 2011 FY- February 2023 FY (blue line) and November 2017FY - January 2023 FY (purple line) (This study). Full time-series indices are shown in bottom figure.